Inorg. Chem. **2006**, *45*, 8584–8596

Synthesis, Structure, and Photophysical Properties of Luminescent Platinum(II) Complexes Containing Cyclometalated 4-Styryl-Functionalized 2-Phenylpyridine Ligands

Biaolin Yin,[§] Felix Niemeyer,[§] J. A. Gareth Williams,*[,‡] Ji Jiang,[§] Abdou Boucekkine,*[,§] Loïc Toupet,[#] Hubert Le Bozec,[§] and Véronique Guerchais*[,§]

UMR CNRS-Université de Rennes 1 6226, Sciences Chimiques de Rennes, Campus de Beaulieu, 35042 Rennes Cedex, France, Department of Chemistry, University of Durham, South Road, Durham, DH1 3LE, United Kingdom, and Groupe Matière Condensée, UMR Université de Rennes 1 6626, Campus de Beaulieu, 35042 Rennes Cedex, France

Received April 28, 2006

A series of new luminescent cyclometalated platinum(II) complexes functionalized with various substituted styryl groups on the cyclometallating ligand [Pt(*C*∧*N*-ppy-4-styryl-R)(*O*∧*O*-(O)CCR′CHCR′C(O))] (ppy-4-styryl-R = *E*-4(4-(R)styryl-2-phenylpyridine) (**3**, R′ = Me (acac); **4**, R′ = ^{t}Bu (dpm); R = H, OMe, NEt_2, NO_2) have been prepared. All complexes undergo an *E*–*Z* photoisomerization process in CH_2Cl_2 solution under sunlight, as monitored by ^{1}H NMR. The solid-state structures of **3-OMe**, **3-NEt$_2$**, **3-NO$_2$**, and **4-OMe** have been determined by X-ray diffraction studies and compare well with optimized geometries obtained by density functional theory (DFT) calculations. The orbital pictures of **3-H**, **3-OMe**, and **3-NO$_2$** are very similar, the highest occupied molecular orbital (HOMO) being highly Pt(5d) metal-based. For **3-NMe$_2$**, an additional contribution from the amino-styryl fragment leads to a decreased metal parentage of the HOMO, suggesting a predominantly ILCT character transition. Complexes **3-H**, **3-OMe**, and **3-NO$_2$** show a low-energy band (350–400 nm) assigned to predominantly charge-transfer transitions. The amino derivative **3-NEt$_2$** displays a very strong absorption band at 432 nm, tentatively assigned to a mixture of ILCT (Et_2N → CH=CH*) and metal-to-ligand charge-transfer (MLCT) (dπ(Pt) → π*) transitions. Complexes **3** are weakly luminescent in CH_2Cl_2 solution at room temperature; the low intensity may be due to a competitive quenching through the *E*–*Z* photoisomerization process. All complexes exhibit similar structured emission bands under these conditions (λ_{em}^{max} around 520 nm), independent of the nature of the styryl-R group. In a frozen EPA glass (77 K), the spectrum of the representative complex **3-H** exhibits two sets of vibronically structured bands (460–560, 570–800 nm; λ_{max} = 596 nm), due to the presence of two emitting species, the *E* and *Z* isomers, which have significantly different triplet excited-state energies. The other three complexes show similar behavior to **3-H** at 77 K, but the lower-energy emission bands are progressively red-shifted in the order H < OMe < NO_2 < NEt_2 (e.g., for **3-NEt$_2$**, λ_{em}^{max} = 658 nm; τ = 26 μs). The very large red-shift compared to related unsubstituted complexes (e.g., to [Pt(*C*∧*N*-ppy)(*O*∧*O*-acac)]) is the result of the extension of the π-conjugated system and the electronic effects of substituent R.

Introduction

A significant research effort has focused on the design and photophysical properties of third-row transition metal complexes. These complexes often exhibit high quantum yields of phosphorescent emission from triplet excited states, due to the mixing of the singlet and triplet states promoted by the high spin−orbit coupling constant of the heavy metal ion. Among them, platinum(II) complexes incorporating polypyridine ligands such as bipyridine and terpyridine derivatives have attracted a great deal of interest as luminescent chromophores for potential applications in the conversion of light to chemical energy (artificial photosyn-

* To whom correspondence should be addressed. E-mail: j.a.g.williams@durham.ac.uk (J.A.G.W.); abdou.boucekkine@univ-rennes1.fr (A.B.); veronique.guerchais@univ-rennes1.fr (V.G.).
[§] UMR CNRS 6226, Sciences Chimiques.
[#] UMR CNRS 6626, Université de Rennes 1.
[‡] University of Durham.

10.1021/ic0607282 CCC: $33.50
Published on Web 09/13/2006

thesis), organic light-emitting devices (OLEDs), or biological labels.[1−3] In recent years, several cyclometalated homo- or heteroleptic platinum(II) complexes based on 2-phenylpyridine (ppy) and analogues have been reported in the literature.[4−7] They generally feature long-lived excited states in frozen glasses and/or solutions that originate from a mixed ^{3}LC-MLCT state (MLCT = metal-to-ligand charge-transfer). These studies also pointed out the crucial importance of cyclometallating ligands that strongly govern the emission characteristics of the complexes in two key ways. First, the very strong ligand field associated with the cyclometallating carbon serves to raise the energy of the strongly antibonding, metal-centered excited state formed through population of the $d_{x^2-y^2}$ orbital. When thermally accessible at room temperature, as it is in Pt(bpy)Cl_2, for example, this state provides a deleterious pathway of nonradiative decay,[1a,8] but by raising its energy in cyclometalated complexes, its influence is attenuated leading to greatly increased quantum yields.[4−7,9] Second, emission color tuning, from blue-green to orange-red, can be achieved through rational modification of the ppy ligand with electron-donating or -withdrawing substituents or π-conjugated groups. For instance, quite large phosphorescence red-shifts were observed at 77 K upon extending the size of the π-conjugated system of the $C\wedge N$ ligand. Thus, the emission shifts from green for Pt($C\wedge N$-ppy)($O\wedge O$-dpm) to orange-red for Pt($C\wedge N$-pq)($O\wedge O$-dpm) (λ_{em}^{max} $_{77\ K}$ = 477 and 555 nm, respectively; dpm = dipivolylmethane, pq = 2-phenylquinoline).[7]

For the past 10 years, our laboratory has focused on studying the nonlinear optical properties of tris(dialkylaminostyryl-2,2′-bipyridine)metal complexes.[10] These chromophores display intense low-lying ILCT and MLCT transitions in absorption, both of which contribute to the NLO activity. In addition, the ruthenium(II) complex also shows relatively long-lived luminescence (>5 μs) at an emission maximum of 708 nm, corresponding to a large bathochromic shift of almost 100 nm with respect to $[Ru(bpy)_3]^{2+}$.[11] More recently, we have investigated the photophysical properties of tris-cyclometalated iridium(III) complexes Ir($C\wedge N$)$_3$ based on the new 4-(4-(donor)styryl-2-phenylpyridine ligands (donor, D = OMe, NEt_2).[12] Again, a large bathochromic shift up to 158 nm with respect to Ir(ppy)$_3$ was observed in their emissions at 77 K (D = OMe, λ_{em} = 616 nm; D = NEt_2, λ_{em} = 650 nm), originating from a switch to a ^{3}ILCT emissive excited state. Thus, in these two families of complexes, the red-shift is a result of the donor substituent in addition to the extension of conjugation (styryl).

In the present study, we focus on the preparation and photophysical studies of a series of cyclometalated platinum(II) complexes of the general formula Pt($C\wedge N$)($O\wedge O$), where $O\wedge O$ is either acetylacetonate (acac) or dipivolylmethane (dpm), and $C\wedge N$ represents 4-styryl-2-phenylpyridine ligands para-substituted by different groups R, from strongly withdrawing to strongly donating substituents (R = NO_2, H, OMe, NEt_2).

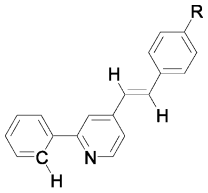

R = NO_2, H, OMe, NEt_2

The purpose of this study was to determine how the emitting state of the Pt complex is influenced by the presence of a -CH=CH−Ar styryl substituent in the 4-position of the pyridine ring and, moreover, whether further tuning of the

(1) (a) Miskowski, V. M.; Houlding, V. H.; Che, C.-M.; Wang, Y. *Inorg. Chem*. **1993**, *32*, 2518. (b) Bevilacqua, J.; Eisenberg, R. *Inorg. Chem.* **1994**, *33*, 2913. (c) Hissler, M.; Connick, W. B.; Geiger, D. K.; McGarrah, J. E.; Lipa, D.; Lachicotte, R. J.; Eisenberg, R. *Inorg. Chem.* **2000**, *39*, 447. (d) Hissler, M.; McGarrah, J. E.; Connick, W B.; Geiger, D. K.; Cummins, S. D.; Eisenberg, R. *Coord. Chem. Rev.* **2000**, *208*, 115. (e) Chan, S.-C.; Chan, M. C. W.; Wang, Y.; Che, C.-M.; Cheung, K. K.; Zhu, N. *Chem. Eur. J.* **2001**, *7*, 4180. (f) Whittle, C. E.; Weinstein, J. A.; George, M. W.; Schanze, K. S. *Inorg. Chem*. **2001**, 40, 4053. (g) Siu, P. K. M.; Lai, S.-W.; Lu, W.; Zhu, N.; Che, C.-M. *Eur. J. Inorg. Chem.* **2003**, 2749. (h) Makedonas, C.; Mitsoupolous, C. A.; Lahoz, F. J.; Balana, A. I. *Inorg. Chem.* **2003**, *42*, 8853. (i) Lu, W.; Chan, M. C. W.; Zhu, N.; Che, C.-M.; Wong, K.-Y. *Chem. Eur. J.* **2003**, *9*, 6155. (j) Lui, Q.-D.; Wang, R.; Wang, S. *J. Chem. Soc., Dalton Trans*. **2004**, 2073. (k) Kinayyigit, S.; Hua, F.; Cable, J. R.; Castellano, F. N. *Inorg. Chem.* **2005**, *44*, 471. (l) Danilov, E. O.; Pomestchenko, I. E.; Kinayyigit, S.; Gentili, P. L.; Hissler, M.; Ziessel, R.; Castellano, F. N. *J. Phys. Chem. A.* **2005**, *109*, 2465.

(2) (a) Yam, V. W−W.; Wong, K. M.-C.; Zhu, N. *J. Am. Chem. Soc*. **2002**, *124*, 6506. Millin, D. R.; Moore J. J. *Coord. Chem. Rev*. **2002**, *229*, 113. (b) Wong, K. M.-C.; Tang, W.-S.; Chu, B. W.-K.; Zhu, N.; Yam, V. W.-W. *Organometallics* **2004**, *23*, 3459. (c) Wong, K. M.-C.; Tang, W.-S.; Lu, X.-X.; Zhu, N.; Yam, V. W.-W. *Inorg. Chem.* **2005**, *44*, 1492. (d) Yam, V. W.-W., Chan, K. H.-Y.; Wong, K. M.-C.; Zhu, N. *Chem. Eur. J.* **2005**, *11*, 4535. (e) Ma, D. L.; Shum, T. Y. T.; Zhang, F.; Che, C. M.; Yang, M. *Chem. Comm*. **2005**, 4675. (f) Guo, F.; Sun, W.; Liu, Y.; Schanze, K. *Inorg. Chem.* **2005**, *44*, 4055.

(3) (a) Baldo, M. A.; O'Brien, D. F. You, Y.; Shoustikov, Sibley, S.; Thompson, M. E.; Forrest, S. R. *Nature* **1998**, *395*, 151. (b) Kwong, R. C.; Sibley, S.; Dubovoy, T.; Baldo, M. A.; Forrest, S. R.; Thompson, M. E. *Chem. Mater*. **1999**, *11*, 3709. (c) O'Brien, D. F.; Baldo, M. A.; Thompson, M. E.; Forrest, S. R. *Appl. Phys. Lett.* **1999**, *74*, 442. (d) Adachi, C.; Baldo, M. A.; Forrest, S. R.; Lamansky, S.; Thompson, M. E.; Kwong, R. C. *Appl. Phys. Lett*. **2001**, *78*, 1622. Cleave, V.;. Yahioglu, G.; Barny, P. L.; Friend, R. H.; Tessler, N. *Adv. Mater*. **1999**, *11*, 285. (e) D'andrade, B. W.; Brooks, J.; Adamovich, V.; Thompson, M. E.; Forrest, S. R. *Adv. Mater*. **2002**, *14*, 1032. (f) Adamovich, V.; Brooks, J.; Tamayo, A.; Alexander, A. M.; Djurovich, P. I.; D'Andrade, B. W.; Adachi, C.; Forrest, S. R.; Thompson, M. E. *New J. Chem.* **2002**, *26*, 1171. (g) Kwok, C.-C.; Ngai, H. M. Y.; Chan, S.-C.; Sham, I. H. T.; Che, C.-M.; Zhu, N. *Inorg. Chem.* **2005**, *44*, 4442. (h) Kavitha, J.; Chang, S.-Y.; Chi, Y.; Yu, J.-K.; Hu, Y.-H.; Chou, P.-T.; Peng, S.-M.; Lee, G.-H.; Tao, Y.-T.; Chien, C.-H.; Carty, A. *Adv. Funct. Mater*. **2005**, *15*, 223. (i) Wong, W.-Y.; He, Z.; So, S.-K.; Tong, K.-L.; Lin, Z. *Organometallics* **2005**, *24*, 4079. (j) Chang, S.-Y.; Kavitha, J.; Li, S.-W., Hsu, C.-S.; Chi, Y.; Yeh, Y.-S.; Chou, P.-T.; Lee, G.-H.; Carty, A. J., Tao, Y.-T.; Chien, C.-H. *Inorg. Chem.* **2006**, 45, 137.

(4) (a) Chassot, L.; Muller, E.; von Zelewsky, A. *Inorg. Chem.* **1984**, 23, 4249. (b) Jolliet, P.; Gianini, M.; von Zelewsky, A.; Bernardinelli, G.; Stoeckli-Evans, H. *Inorg. Chem*. **1996**, *35*, 4883.

(5) (a) Craig, C. A.; Garces, F. O.; Watts, R. J.; Palmans, R.; Frank, A. J. *Coord. Chem. Rev.* **1990**, *97*, 193. (b) Mdleleni, M. M.; Bridgewater, J. S.; Watts, R. J.; Ford, P. C. *Inorg. Chem.* **1995**, *34*, 2334.

(6) (a) Balashev, K. P.; Puzyk, M. V., Kotlyar, V. S.; Kulikova, M. V. *Coord. Chem. Rev.* **1997**, *159*, 109. (b) Yersin, H.; Donges, D.; Humbs, W.; Strasser, J.. Sitters, R.; Glasbeek, M. *Inorg. Chem.* **2002**, *41*, 4915. (c) Kunugi, Y.; Mann, K. R.; Miller, L. L.; Exstrom, C. L. *J. Am. Chem. Soc*. **1998**, *120*, 589. (d) Lu, W.; Mi, B.-X.; Chan, M. C. W.; Hui, Z.; Zhu, N.; Lee, S.-T.; Che, C.-M. *Chem. Commun*. **2002**, 206.

(7) Brooks, J.; Babayan, Y.; Lamansky, S.; Djurovich, P. I.; Tsyba, I.; Bau, R.; Thompson, M. E. *Inorg. Chem*. **2002**, *41*, 3055.

(8) Aldridge, T. K.; Stacy, E. M.; McMillin, D. R. *Inorg. Chem.* **1994**, *33*, 722.

Scheme 1

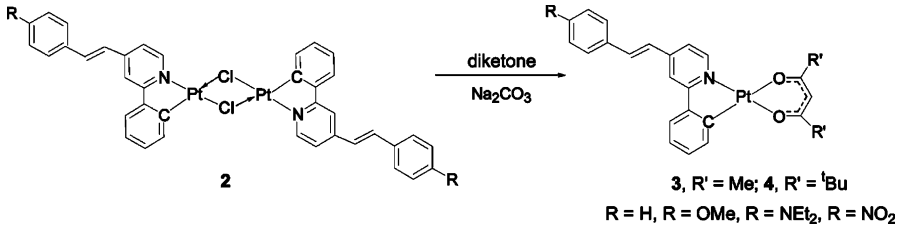

emission energy and properties could be achieved according to the presence of electron-donating (e.g., NEt_2) or electron-withdrawing (e.g., NO_2) end substituents R in the styryl phenyl ring. In an attempt to rationalize the electronic modifications induced by the substituents and to elucidate the nature of the excited states involved, density functional theory (DFT) calculations on the acac series of complexes were carried out.

Results and Discussion

Syntheses. The synthesis of the styryl ligands **1** was achieved following the procedures reported for the related bipyridine ligands,[13] i.e., either by a Knoevenagel-type condensation between the appropriate aldehydes (R = H, OMe, NEt_2) and 4-methyl-2-phenylpyridine or (for R = NO_2) by means of a Wadworth−Emmons reaction between *p*-nitrobenzaldehyde and 4-diethylphosphonatomethyl-2-phenylpyridine.[14] The complexes Pt(*C*∧*N*-ppy-4-styryl-R)[*O*∧*O*-(O)CCR′CHCR′C(O)] (ppy-4-styryl-R = (*E*-4-(4-R-styryl-2-phenylpyridine) (**3**, R′ = CH_3; **4** R′ = ^{t}Bu; R = H, OMe, NEt_2, NO_2) were synthesized by employing a two-step procedure previously reported for Pt(*N*∧*C*)(*O*∧*O*) complexes.[7] Treatment of K_2PtCl_4 with 3 equiv of H*C*∧*N* (**1**) afforded the chloro-bridged dimers **2**,[15] which were subsequently converted into the oxygenated acac (**3**) or dpm (**4**) derivatives, upon treatment with the appropriate diketone (acetylacetone, dimethylpivaloylmethane) in the presence of Na_2CO_3 in 2-ethoxyethanol (80 °C) (Scheme 1). Complexes **3** and **4** were isolated as air-stable yellow-orange crystals in moderate yield (30−50%), the crude product being contaminated by the free ligand H*C*∧*N*. They were purified by crystallization from a mixed dichloromethane/ethanol solution.

All complexes have been fully characterized by ^{1}H and ^{13}C NMR spectroscopy. The ^{1}H NMR spectra show characteristic platinum satellites (^{195}Pt, I = $^1/_2$, 33.8% natural abundance). For instance, the proton in the 6-position of the pyridine ring of **3-OMe** appears as a low-field doublet at δ 8.91 (CD_2Cl_2: $^3J_{H-H}$ = 6 Hz, $^3J_{Pt-H}$ = 41 Hz). The AB system located at δ 7.44 and 7.00 ($^3J_{H-H}$ = 16 Hz) confirms the presence of the *E*-styryl group. In the ^{13}C NMR spectrum, the =CH signals appear at δ 134.7 and 122.6. The CH resonance of the acac ligand is located typically at 5.54 (δ^{13}C = 102.3).

It is noteworthy that these compounds can undergo *E*−*Z* isomerization of the C=C double bond of the styryl group, upon exposure to sunlight or in the presence of traces of acid. Thus, irradiation of a CD_2Cl_2 solution (10^{-3} M, λ_{ex} = 350 nm) led to a mixture of *Z* (62%) and *E* (38%) isomers after 3 h: a second AB system was then observed at δ 6.91 and 6.49 ppm, with a coupling constant $^3J_{H-H}$ of 12 Hz, typical for a *Z* configuration double bond (Figure 1). This ratio represents the equilibrium state for **3-OMe** at this wavelength, showing no further change upon continued irradiation. Interestingly, such isomerization has never been observed for the related metal 4-styryl-bipyridine (*N*∧*N*-coordinated) complexes.[11,13a]

Crystal Structures. The molecular structures of **3-OMe**, **4-OMe**, **3-NEt_2**, and **3-NO_2** were determined by X-ray diffraction studies (Figures 2−5), confirming the *E* configuration of the styryl group in each case. Selected bond lengths and angles are listed in Table 1. In all molecules, the platinum center exhibits the expected square planar coordination and the ppy metallacycle is essentially flat. In the acac derivatives **3-OMe** and **3-NEt_2**, the R-styryl group is not coplanar with the plane of the ppyPt(acac) fragment; the torsion angles are 18.4° (C13−C14−C17−C18) and 16.9° (C8−C9−C12−C13), respectively. The NO_2 group of **3-NO_2** is slightly distorted (C16−C17−N2−O3: 10.39°). All these deviations may be due to the packing forces existing in the crystal. The metal−atom distances in **3-NEt_2** are shorter than those of the methoxy derivative **3-OMe**, suggesting stronger bonds, and similarly in the dpm adduct **4-OMe**. In complex **3-NO_2**, a slight lengthening of the distances is observed. The two Pt−O bond lengths are different, the longer of the two consistently being that disposed trans to the cyclometallating carbon. This is a reflection of the trans influence of the phenyl ligand, a feature observed for other chelating diketonato complexes containing bidentate cyclometallating ligands.[7,16] The bite N−Pt−C angles are similar to those found for related (*C*∧*N*)Pt complexes.[7,16] Molecules of **4-OMe** pack as head-to-tail dimers with a plane-to-plane

(9) (a) Lai, S. W.; Chan, M. C. W.; Cheung, T.-C.; Peng, S.-M.; Che, C.-M. *Inorg. Chem.* **1999**, *38*, 4046. (b) Che, C.-M.; Fu, W.-F.; Lai, S.-W.; Hou, Y.-J.; Liu, Y.-L. *Chem. Commun.* **2003**, 118. (c) Lu, W.; Mi, B.-X.; Chan, M. C. W.; Hui, Z.; Che, C.-M. Zhu, N.; Lee, S.-T. *J. Am. Chem. Soc.* **2004**, *126*, 4958. (d) Yang, Q.-Z.; Wu, L.-Z.; Zhang, H.; Chen. B.; Wu, Z.-X.; Zhang, U.-P.; Tung, C.-H. *Inorg. Chem.* **2004**, *43*, 5195. (e) Williams, J. A. G.; Beeby; A.; Davies, E. S.; Weinstein, J. A.; Wilson, C. *Inorg. Chem*. **2003**, *42*, 8609. (f) Farley, S. J.; Rochester, D. L.; Thompson, A. L.; Howard, J. A. K. Williams, J. A. G. *Inorg. Chem.* **2005**, *44*, 9690. (g) Fernandez, S.; Forniès, J.; Gil, B.; Gomez, J.; Lalinde, E. *Dalton Trans*. **2003**, 822.
(10) Maury, O.; Le Bozec, H. *Acc. Chem. Res*. **2005**, *38*, 691.
(11) Le Bouder, T.; Maury, O.; Bondon, A.; Costuas, K.; Amouyal, E.; Ledoux, I.; Zyss, J.; Le Bozec, H. *J. Am. Chem. Soc.* **2003**, *125*, 12284.
(12) Lepeltier, M.; Le Bozec, H.; Guerchais, V.; Lee, T. K.-M.; Lo, K. K.-W. *Organometallics* **2005**, *24*, 6069.
(13) (a) Maury, O.; Guégan, J.-P.; Renouard, T.; Hilton, A.; Dupau, P.; Sandon, N.; Toupet, L.; Le Bozec, H. *New J. Chem.* **2001**, *25*, 1553. (b) Viau, L.; Maury, O.; Le Bozec, H. *Tetrahedron Lett.* **2004**, *45*, 125.
(14) Lepeltier, M. Ph.D. thesis, Université de Rennes 1, 2005.
(15) (a) Cockburn, B. N.; Howe, D. V.; Keating, T.; Johnson, B. F. G.; Lewis, J. *J. Chem. Soc., Dalton Trans.* **1973**, 404.

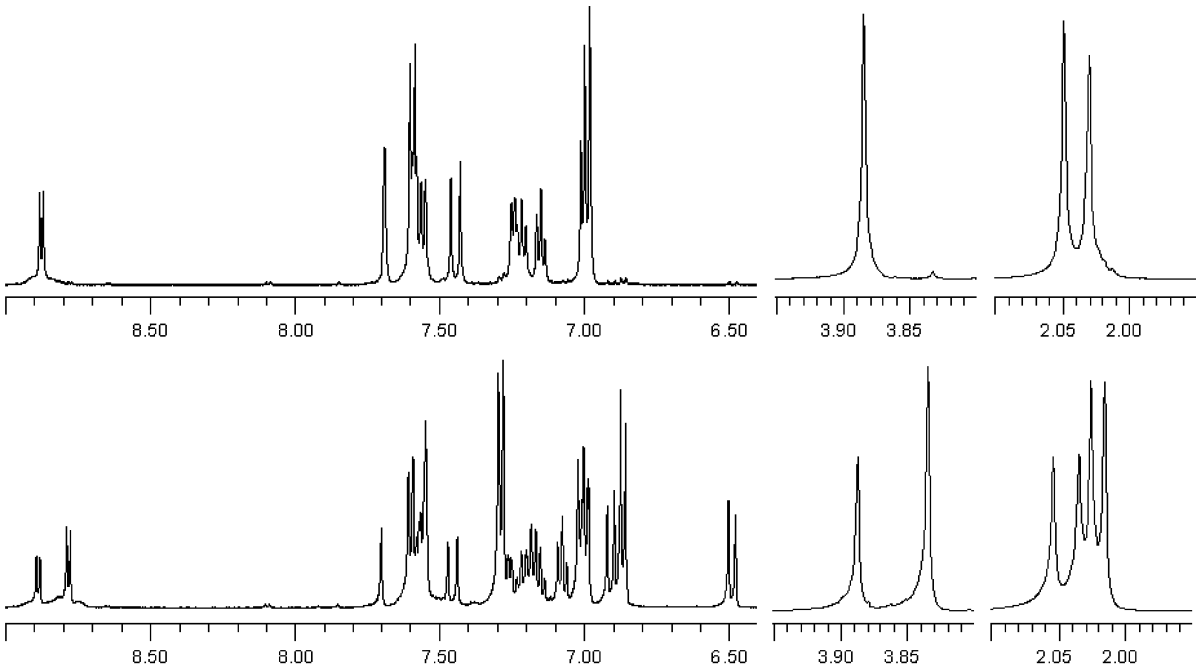

Figure 1. ^{1}H NMR spectra (CD_2Cl_2) of **3-OMe**, before (top) and after (bottom) UV irradiation for 3 h (λ = 350 nm, 10^{-3} M).

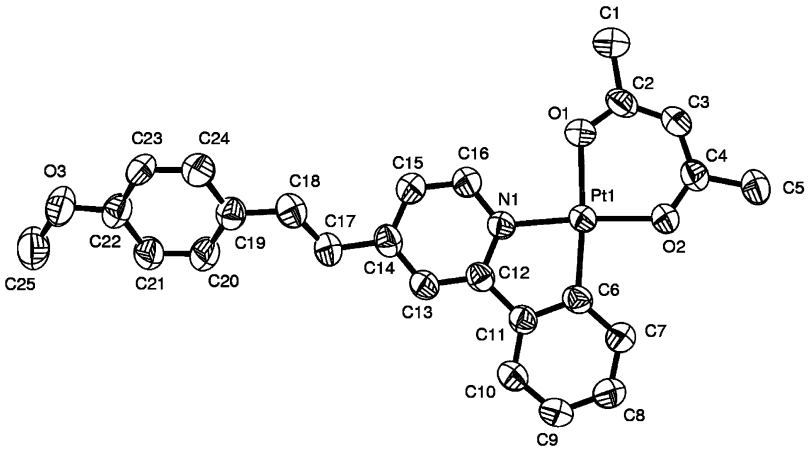

Figure 2. Diagram ORTEP (293 K, 50% probability thermal ellipsoids) of complex **3-OMe**. Hydrogen atoms are omitted for clarity.

separation of 4.07 Å, a distance that is too long for a $\pi-\pi$ stacking interaction.[16] In this case, the ppy-4-styryl-OMe ligand is almost planar (dihedral angle < 10°), probably because of the sterically demanding nature of the ^{t}butyl substituents.

DFT Calculations (1): Optimized Geometries. DFT calculations were carried out on the electronic ground state of Pt(*C*∧*N*-ppy-4-styryl-R)(*O*∧*O*-acac) featuring **H**, **OMe**, **NO_2**, and **NMe_2** (as a smaller model of **NEt_2**), using BP86 and LB94 DFT (see computional details). The calculated ground-state structures (BP86) are in good agreement with those determined for **3-OMe**, **3-NO_2**, **and 3-NEt_2** by X-ray diffraction studies. Selected optimized bond lengths and angles are given in Table 2. The platinum center exhibits the expected square-planar geometry, and the ppy fragment is essentially flat (largest deviation from the main plane defined by the metallacycle atoms: 2.97°). In agreement with the experimental structure, the styryl group deviates from the plane of the metallacycle for **3-OMe** and **3-NMe_2** (torsion angles 16.9° and 17.5°, respectively). Irrespective of the identity of the substituent R, the bond lengths are slightly shorter than those calculated for [Pt(*C*∧*N*-ppy)(*O*∧*O*-acac)] (**1**).[7]

Electronic Absorption Spectra. The electronic absorption spectra of the two series of complexes **3** and **4** were recorded in CH_2Cl_2 solution at 298 K, and data are summarized in Table 3. The spectra of the dpm complexes **4** were almost identical to those of the corresponding acac derivatives **3**

(16) (a) Ionkin, A. S.; Marshall, W. J.; Wang, Y. *Organometallics* **2005**, *24*, 619. (b) Giordano, T. J.; Rasmussen, P. G. *Inorg. Chem.* **1975**, *14*, 1628. (c) Breu, J.; Range, K.-J.; von Zelewsky, A.; H. Yersin, H. *Acta Crystallogr.* **1997**, *C53*, 562. (d) Ghedini, M.; Pucci, D.; Crispini, A.; Barberio, G. *Organometallics* **1999**, *18*, 2116. (e) Mdleleni, M. M.; Bridgewater, J. S.; Watts, R. J.; Ford, P. C. *Inorg. Chem.* **1995**, *34*, 2334. (f) DePriest, J.; Zheng, G. Y.; Woods, C.; Rillema, D. P.; Mikirova, N. A.; Zandler, M. E. *Inorg. Chim. Acta* **1997**, *264*, 287. (g) DePriest, J.; Zheng, G. Y.; Goswami, N.; Eichhorn, D. M.; Woods, C.; Rillema, D. P. *Inorg. Chem.* **2000**, *39*, 1955.

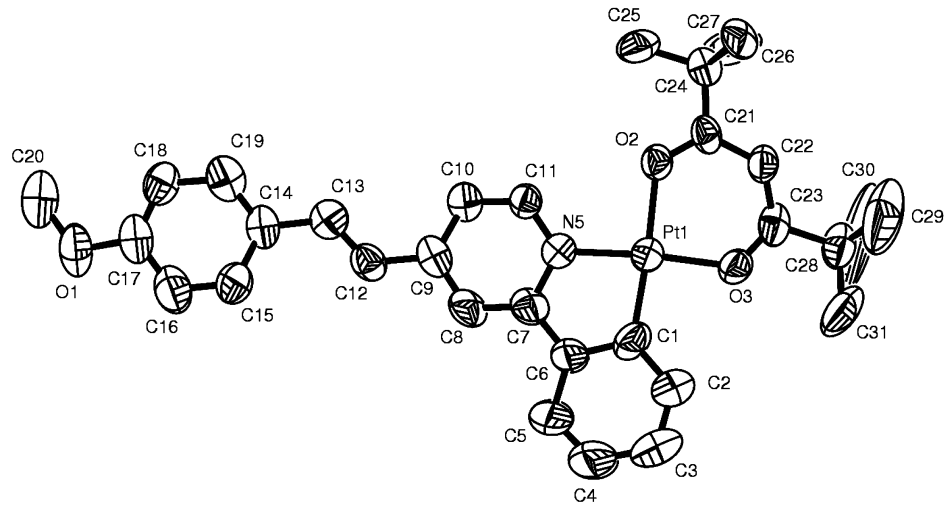

Figure 3. Diagram ORTEP (293 K, 50% probability thermal ellipsoids) of complex **4-OMe**. Hydrogen atoms are omitted for clarity.

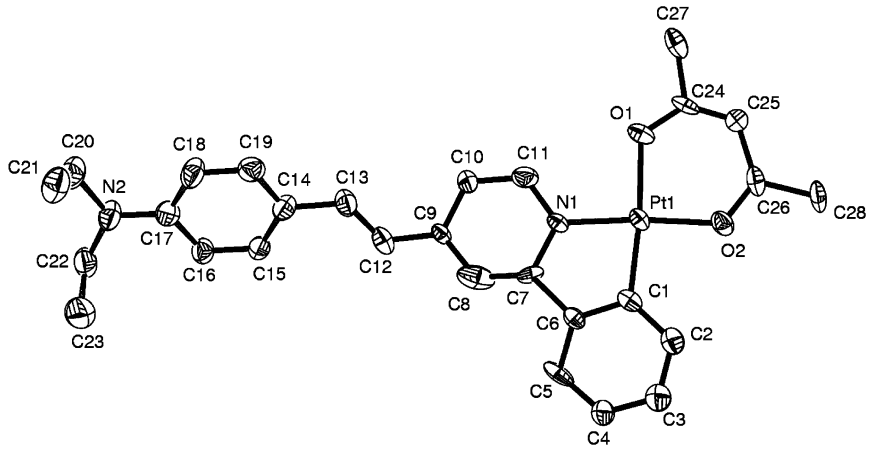

Figure 4. Diagram ORTEP (120 K, 50% probability thermal ellipsoids) of complex **3-NEt**$_2$. Hydrogen atoms are omitted for clarity.

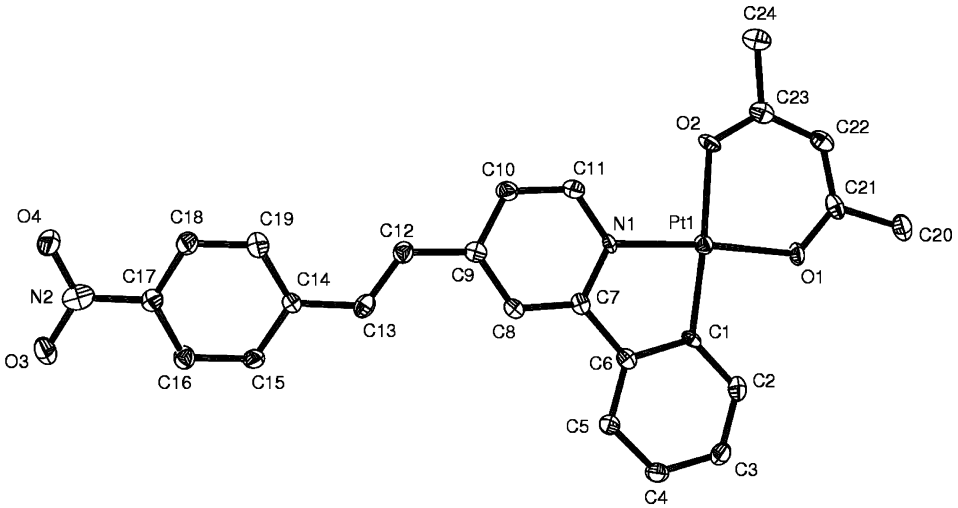

Figure 5. Diagram ORTEP (120 K, 50% probability thermal ellipsoids) of complex **3-NO**$_2$. Hydrogen atoms are omitted for clarity.

with only small shifts observed in some bands, a feature that has previously been observed in the parent ppy and 2-thienylpyridine (thpy) complexes Pt(*C*∧*N*)(*O*∧*O*).[7] Only for the amino derivative are the differences in wavelengths between the dpm and acac derivatives significant. In considering the effect of the styryl substituents, therefore, we shall confine the following discussion to the acac series of complexes.

The absorption spectra of the four acac complexes are shown in Figure 6. The spectrum of the unsubstituted styryl compound (**3-H**) displays a very strong band in the UV (λ_{max} = 316 nm, ϵ = 27750) and a second band of about half the intensity tailing well into the visible region (λ_{max} = 392 nm, ϵ = 12960). The spectra of the *p*-nitro- and *p*-methoxy-styryl analogues (**3-NO**$_2$ and **3-OMe**) are very similar to that of

Table 1. Selected Bond Distances (Å) and Angles (deg) for Complexes **3-OMe**, **4-OMe**, **3-NEt$_2$**, and **3-NO$_2$**

Pt(*C*∧*N*-ppy-4-styryl-OMe)(acac) **3-OMe**			
Pt(1)−O(2)	2.000(3)	Pt(1)−O(3)	2.089(3)
Pt(1)−N(1)	1.984(3)	Pt(1)−C(6)	1.970(4)
C(17)−C(18)	1.330(6)		
O(1)−Pt(1)−O(2)	91.60(13)	O(1)−Pt(1)−N(1)	93.11(4)
O(2)−Pt(1)−N(1)	175.28(13)	O(1)−Pt(1)−C(6)	174.70(15)
O(2)−Pt(1)−C(6)	93.69(16)	N(1)−Pt(1)−C(6)	81.60(17)
Pt(*C*∧*N*-ppy-4-styryl-NEt$_2$)(acac) **3-NEt$_2$**			
Pt(1)−O(2)	1.988(9)	Pt(1)−O(1)	2.073(8)
Pt(1)−N(1)	1.968(10)	Pt(1)−C(1)	1.966(12)
C(12)−C(13)	1.33 (2)		
O(1)−Pt(1)−O(2)	91.7(4)	O(2)−Pt(1)−N(1)	174.9(4)
O(1)−Pt(1)−N(1)	93.4(4)	O(1)−Pt(1)−C(1)	173.9(5)
O(2)−Pt−C(1)	94.1(4)	N(1)−Pt−C(1)	80.9(5)
Pt(*C*∧*N*-ppy-4-styryl-OMe)(dpm) **4-OMe**			
Pt(1)−O(2)	1.992(7)	Pt(1)−O(3)	2.075(7)
Pt(1)−N(5)	1.980(8)	Pt(1)−C(1)	1.958(13)
C(12)−C(13)	1.299(14)		
O(2)−Pt(1)−O(3)	91.6(3)	O(3)−Pt(1)−N(5)	171.4(13)
O(2)−Pt(1)−N(5)	93.4(3)	O(2)−Pt(1)−C(1)	174.6(16)
O(3)−Pt(1)−C(1)	92.3(3)	N(5)−Pt(1)−C(1)	82.2(4)
Pt(*C*∧*N*-ppy-4-styryl-NO$_2$)(acac) **3-NO$_2$**			
Pt(1)−O(1)	2.011(5)	Pt(1)−O(2)	2.093(6)
Pt(1)−N(1)	1.988(6)	Pt(1)−C(1)	1.963(7)
C(12)−C(13)	1.333(12)		
O(1)−Pt(1)−O(2)	91.7(2)	O(1)−Pt(1)−N(1)	174.9(2)
O(2)−Pt(1)−N(1)	93.4(2)	O(2)−Pt(1)−C(1)	175.2(3)
O(1)−Pt(1)−C(1)	92.8(3)	N(1)−Pt(1)−C(1)	82.1(3)

3-H but with a red-shift in the higher energy band (to λ_{max} 333 and 336 nm, respectively). Meanwhile, the low-energy band is slightly red-shifted in **3-NO$_2$** and blue-shifted in **3-OMe**. By comparison with the absorption properties of [Pt(*C*∧*N*-ppy)(*O*∧*O*-acac)], the former is most likely due to intraligand $\pi-\pi^*$ transitions, while the lower energy bands could tentatively be assigned to MLCT ($d\pi(Pt) \rightarrow \pi^*$) transitions, which typically occur in this region for cyclometalated complexes and are responsible for the colors of the complexes.[4−7]

In contrast, the absorption spectrum of the amino-substituted complex, **3-NEt$_2$**, is markedly different, displaying a very strong low-energy absorption band at 432 nm (ϵ 24360). This band probably arises from the influence of the strongly electron-donating nature of the amino group and its relative ease of oxidation favoring the formation of a charge-separated excited state. In fact, the profound effect of the amino substituent is also seen in the behavior of the corresponding uncoordinated ligand ppy-CH═CH−C$_6$H$_4$−NEt$_2$, which displays a low energy, positive solvatochromic absorption band (λ_{max} = 387 nm in CH_2Cl_2), a feature not observed in the other ligands.[14,17] The 45 nm red-shift in this band upon complexation to platinum(II) can be attributed to the enhancement of the π-acceptor character of the pyridine ligand upon coordination to the metal ion, lowering the ILCT energy, an effect also observed in several other amino-substituted polypyridyl ligands upon binding to cat-

(17) Lepeltier, M.; Lee, T. K.-M.; Lo, K. K.-W.; Le Bozec, H.; Guerchais, V. unpublished results.

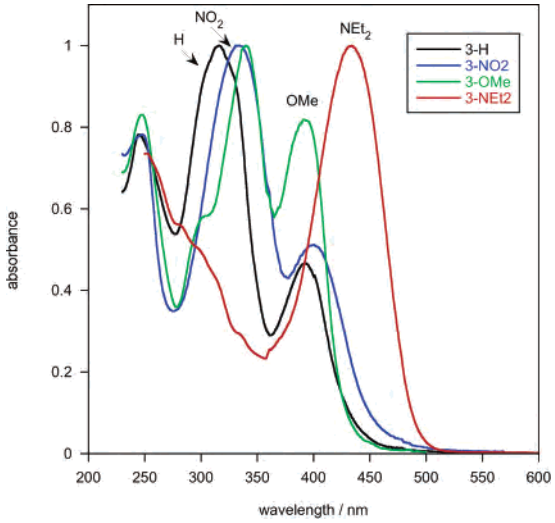

Figure 6. Normalized absorption spectra of **3-H** (black), **3-NO$_2$** (blue), **3-OMe** (green), and **3-NEt$_2$** (red), in CH_2Cl_2 solution at 298 K.

ionic metal centers.[11,13a,18] One or more bands due to MLCT transitions would be anticipated at around 400 nm, as in the other complexes, but these are probably not resolved due to overlap with the ILCT band that obscures them.

DFT Calculations (2): Orbital Parentage of Absorption Bands. The DFT calculations performed on **3-H**, **3-OMe**, **3-NO$_2$**, and **3-NMe$_2$** have allowed the tentative orbital parentage of the transitions giving rise to the observed absorption bands to be largely confirmed. The three highest occupied molecular orbitals (HOMO) and lowest unoccupied molecular orbitals (LUMO) obtained from the calculations are shown in Figure 7, and the relative composition of the different energy levels are reported in Table 4. The nature of the frontier orbitals changes as a function of the nature of R. The valence orbitals of **3-H** and **3-OMe** are very similar to one another: the HOMO is a mixture of Pt(5d$_{yz}$) (42 and 41%, respectively), cyclometalated phenyl, and acac π orbitals, while the LUMO is mainly localized on the "pyridine-CH═CH-" moiety of the styrylpyridine ligand. The HOMO-1 is delocalized over the styryl-C$_6$H$_4$−OMe part of the molecule. The HOMO of **3-NO$_2$** is similar to that of **3-H** and **3-OMe**, again with substantial metal character {Pt(5d), 38%}, combined with π phenyl and acac orbitals. In this case, however, the nitro-substituent makes a major contribution to the LUMO, which now resides predominantly on the "-CH═CH−C$_6$H$_4$−NO$_2$" moiety, with the pyridyl ring playing a much smaller role.

The picture of the HOMO surface of the dimethylamino derivative **3-NMe$_2$** is very different from those of the other complexes: the HOMO comprises the π orbitals of phenyl and acac but now with a substantial additional contribution from the aminostyryl group. Overall, the metallic character decreases to 21% (d$_{xz}$, d$_{yz}$). In all cases, HOMO-1 to HOMO-4 are predominantly metal-based.

(18) (a) Goodall, W.; Williams, J. A. G. *Chem. Commun.* **2001**, 2514. (b) Leslie, W.; Batsanov, A. S.; Howard, J. A. K.; Williams, J. A. G. *Dalton Trans.* **2004**, 623. (c) Leslie, W.; Poole, R. A.; Murray, P. R.; Yellowlees, L. J.; Beeby, A.; Williams, J. A. G. *Polyhedron* **2004**, *23*, 2769. (d) Roberto, D.; Tessore, F.; Ugo, R.; Bruni, S.; Manfredi, A.; Quici, S. *Chem. Commun.* **2002**, 846.

Table 2. DFT (BP86) Calculated Bond Lengths and Angles for [Pt(*C*∧*N*-ppy-4-styryl-R)(*O*∧*O*-acac)]

	bond length (Å)				angles (°)			
complex	Pt−O	Pt−O	Pt−N	Pt−C	O−Pt−O	O−Pt−C	N−Pt−O	C−Pt−N
1[a]	2.15	2.04	2.03	1.98	90.9			81.2
1	2.140	2.046	2.013	1.990	90.05	94.45	94.07	81.43
3-H	2.127	2.031	2.007	1.981	92.06	93.39	93.62	80.93
3-OMe	2.119	2.031	1.999	1.988	92.37	94.28	92.13	81.22
3-NMe$_2$	2.120	2.035	2.002	1.983	92.27	94.40	92.37	80.94
3-NO$_2$	2.129	2.025	2.006	1.980	92.17	93.15	93.21	81.47

[a] Ref 7, B3LYP calculations

Table 3. UV−Visible Absorption and 77 K Emission of Complexes

complex	λ_{abs}/nm (ϵ/M^{-1} cm^{-1})[a]	λ_{em}/nm (77 K)[b]	τ/μs[b]
3-H	248 (21650), 316 (27750), 392 (12960)	{477, 513, 545} {600, 664, 722}	26
4-H	247 (20070), 318 (27230), 395 (13110)	{473, 508, 539} {596, 658, 718}	27
3-OMe	253 (35130), 289sh (26680), 336 (19230), 386(14120)	{607, 669, 734}	24
4-OMe	251 (31780), 294sh (21320), 335 (19590), 390 (14530)	{610, 733, 742}	29
3-NO$_2$	333 (17330), 400 (8840)	{473, 508, 540} {624, 691, 756}	19
3-NEt$_2$	432 (24360)	{473 (br)} {658, 723, 796}	26
4-NMe$_2$	418 (25120)	{477, 513, 545} {638, 704, 775}	27

[a] In CH_2Cl_2 at 298K. [b] In EPA (diethyl ether/isopentane/ethanol, 2/2/1, v/v); lifetimes refer to the low energy bands.

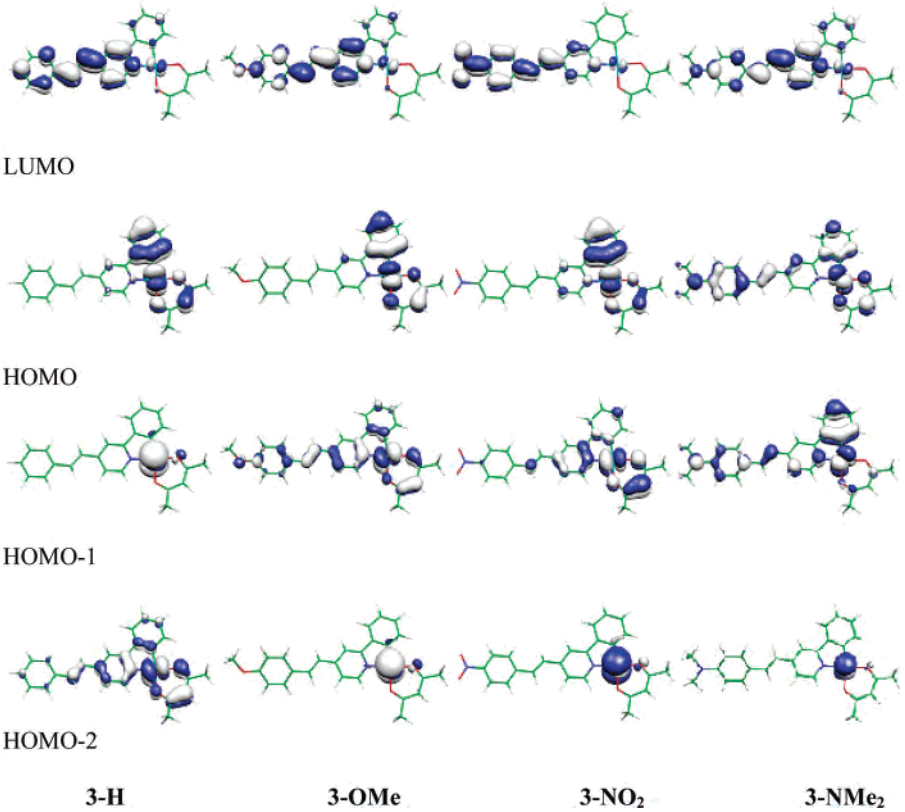

Figure 7. Representations of the valence HOMO and LUMO molecular orbitals obtained from DFT calculations for Pt(*C*∧*N*-ppy-4-styryl-R)[*O*∧*O*-acac], **3-H**, **3-OMe**, **3-NO$_2$**, and **3-NMe$_2$**.

The valence picture that emerges from the DFT calculations is thus one of predominant MLCT/LLCT/IL character for the lowest excited state of **3-H**, **-OMe**, and **-NO$_2$** (we use the abbreviation LLCT for ligand-to-ligand charge transfer, also known as interligand charge transfer, and IL for the intraligand $\pi-\pi^*$ transition of the ppy moiety). The highest occupied orbitals are Pt(5d) in character with ligand π orbitals, and the lowest unoccupied orbitals are π^* ligand in character, styryl-ppy localized for **3-H** and **-OMe**, and nitro-styryl localized for **3-NO$_2$**. In contrast, the lowest excited state of **3-NMe$_2$** has substantial intraligand charge transfer (ILCT) character in addition to MLCT/LLCT contributions, as a result of the large contribution of the $Me_2N-C_6H_4$- moiety to the highest occupied molecular orbital.

Electrochemistry and Solvatochromism. The redox properties of the complexes also reflect the relative electronic influence of the substituent R. Electrochemical studies were performed in DMF ([^{n}Bu$_4$N][PF$_6$] 0.1 M, 100 mV s^{-1}, Pt working electrode, ferrocene as internal reference vs Cp_2-

Table 4. MO Composition[a] (%) for [Pt(*C*∧*N*-ppy-4-styryl-R)(*O*∧*O*-acac)], **3**

	3-H		**3-OMe**		**3-NMe$_2$**		**3-NO$_2$**	
designation	*E* (eV)	Pt(5d)	*E* (eV)	Pt(5d)	*E* (eV)	Pt(5d)	*E* (eV)	Pt(5d)
LUMO+7							−6.38	43
LUMO+6					−5.77	38		
LUMO+5	−6.01	43	−5.96	37				
LUMO+3								
LUMO+1								
LUMO	−8.36		−8.20		−7.91		−9.61	
HOMO	−10.12	42 (d_{yz})	−10.03	41 (d_{yz})	−9.85	21 (d_{yz}, d_{xz})	−10.46	38 (d_{yz})
HOMO-1	−10.31	67(d_{z^2})	−10.24	66 (d_{z^2})	−9.90	30 (d_{yz})	−10.69	67 (d_{z^2})
HOMO-2	−10.35	46 (d_{xz})	−10.27	42 (d_{xz})	−10.08	66 (d_{z^2})	−10.70	40 (d_{xz})
HOMO-3	−10.90	68 (d_{xy})			−10.28	34 (d_{xz})		
HOMO-4			−10.83	68 (d_{xy})	−10.67	69(d_{xy})	−11.27	66 (d_{yz})

[a] LB94 calculations.

Fe/Cp_2Fe^+). The cyclic voltammogram of **3-NO$_2$** displays two reversible waves; the first wave at −1.50 V is attributed to the reduction of the NO_2 group, and the second one at −1.98 V is attributed to that of the *C*∧*N* ligand. The reversible reduction of the *C*∧*N* ligand of **3-H**, **-OMe**, and **-NEt$_2$** are located at −2.00, −2.04, and −2.11 V, respectively, the effect of the amino group being pronounced. The irreversible oxidation of the amino group is observed at 0.40 V. This electrochemical behavior is similar to that reported for (*C*∧*N*)Pt complexes that exhibit a reversible reduction between −1.9 and −2.6 V.[7]

Absorption bands arising from transitions with significant charge-transfer character are often quite strongly solvatochromic.[19] This arises if the CT axis is parallel or roughly parallel with the ground-state dipole, leading to a significant change in the dipole moment in going from the ground to the excited state. In the present instance, **3-NO$_2$** displays the largest effect, exhibiting significant negative solvatochromism {e.g., λ_{max} (solvent) = 410 (toluene), 400 (CH_2Cl_2), 395 (EtOH), 394 nm (MeCN)}, suggestive of an excited state that is significantly less polar than the ground state. In contrast, the absorption band of **3-NEt$_2$** shows very little dependence on the solvent (±4 nm for solvents ranging from toluene to DMSO), and the small effect that is observed does not correlate with the polarity. The absence of solvatochromism of this band could be due to its being comprised of two overlapping transitions, ILCT and MLCT/LLCT, as discussed earlier, giving rise to opposing changes in the polarity. From the DFT perspective, consideration of the frontier orbitals (Figure 7) suggests that formation of the excited state through population of the LUMO will not substantially displace the electron density toward either end of the molecule (the LUMO resides predominantly on the styryl CH=CH π^* unit). Qualitatively, therefore, one might predict rather little change in the dipole moment upon formation of the excited state and therefore little influence of solvent polarity on the absorption energy.

Luminescence. Upon photoexcitation, all members of the two families of complexes **3** and **4** display weak photoluminescence in fluid solution (degassed CH_2Cl_2) at room temperature. As in absorption, the change from acac to dpm has no significant effect on the room-temperature emission properties. The room-temperature emission spectra of series **3** are shown in Figure 8, where it can be seen that all four complexes show very similar spectra to one another, with emission maxima around 520 nm. This represents a significant red-shift compared to the value of 486 nm reported for [Pt(*C*∧*N*-ppy)(*O*∧*O*-acac)] at room temperature[7] (in 2-MeTHF). There is some evidence of structure in the bands, which is most pronounced for the methoxy-substituted complex.

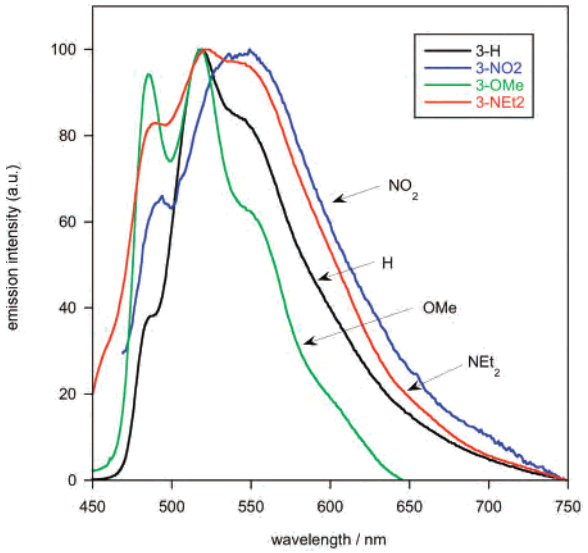

Figure 8. The luminescence emission spectra of **3-H** (black line), **3-OMe** (green), **3-NO$_2$** (blue), and **3-NEt$_2$** (red), in degassed dichloromethane solution at 298 K, following excitation into the lowest energy absorption band; absorption and emission band-passes = 4 nm.

The room-temperature emission intensities are weak in each case: the luminescence quantum yields are in the range of 1×10^{-4} to 2×10^{-3} (CH_2Cl_2) compared to 0.15 for [Pt(*C*∧*N*-ppy)(*O*∧*O*-acac)] (in 2-MeTHF).[7] The weakness of the emission may be due to a competitive quenching through the trans-cis C=C photoisomerization process discussed earlier. Related iridium complexes carrying the -OMe or NEt_2 ligands also displayed very weak emission, where it was noted that hydrogenation of the −CH=CH− bond restored typically strong emission.[12] The similarity in the emission wavelengths of the four complexes to one another in the present case, suggests that, at least at room temperature, the emissive excited state is decoupled from

(19) A detailed discussion of solvatochromism in related platinum(II) complexes is provided by Cummings, S. D.; Eisenberg, R. *J. Am. Chem. Soc.* **1996**, *118*, 1949.

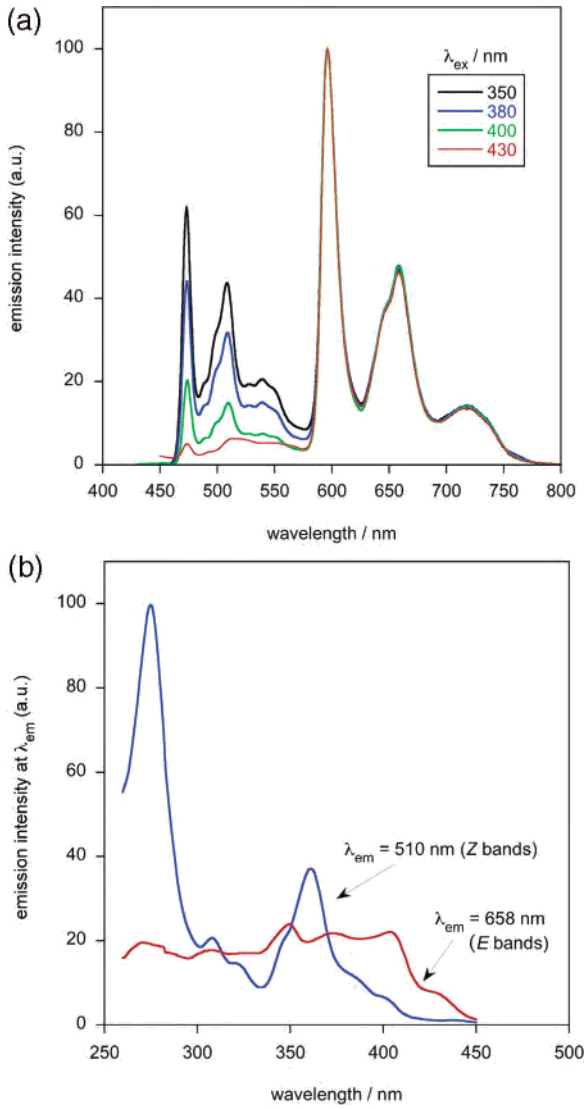

Figure 9. (a) Top: Emission spectra of **3-H** at 77 K in an EPA glass as a function of the excitation wavelength. (b) Bottom: Excitation spectra of **3-H** under these conditions, registered at the wavelength of emission of the second member of the vibrational progression of the two sets of bands (viz. 510 and 658 nm).

the styryl pendent group and involves only the Pt(ppy) moiety. A possible explanation is that the emission at room-temperature emanates from a conformational form containing a half-twisted styryl −CH═CH− unit (the intermediate between trans and cis) that is unconjugated with the ppy ligand.

Luminescence at 77 K. Emission spectra at 77 K were recorded in a frozen EPA glass (EPA = diethyl ether, isopentane, and ethanol, 2/2/1 by volume, with excellent glass-forming characteristics and a very low propensity to cracking). The spectra are very different from those observed at room temperature, and the behavior of **3-H** at 77 K is representative (Figure 9). The spectrum consists of two sets of bands with very well-defined structure, one in the region 460−560 nm and the second set at substantially lower energy in the region 570−800 nm. The two sets of bands have similar profiles, with a vibrational spacing of around 1500 cm^{-1} probably associated with the C═C vibrations, aromatic breathing modes and acac C−O bonds, all with vibrational

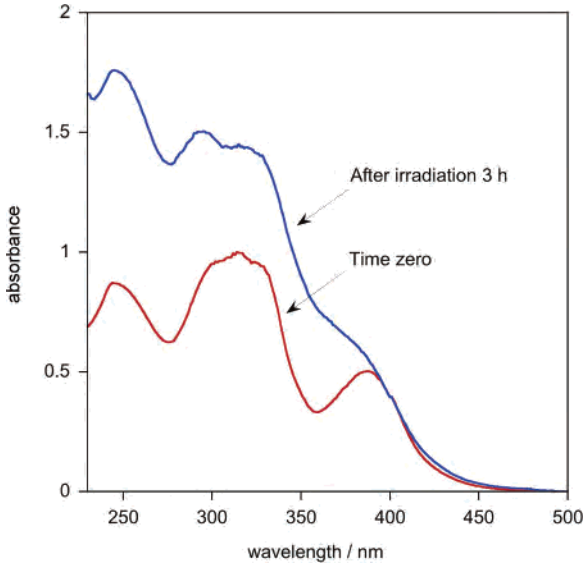

Figure 10. The UV−visible absorption spectra of **3-H** (5×10^{-5} M) in CH_2Cl_2 solution at 298 K before (red line) and after irradiation at 365 nm, 30 W (blue line). Spectra are normalized at 400 nm to highlight the different profiles in the near-UV region.

stretching frequencies of this order. Some additional fine structure is also discernible, common to both sets of bands.

The ratio of the intensity of the higher energy set of bands to those at lower energy is found to be dependent upon the excitation wavelength employed (Figure 9a). This is also evident from the excitation spectra registered at 510 and 658 nm (the maxima of the second member of the vibrational progression of the two sets of bands): their profiles are markedly different (Figure 9b). This suggests that, at 77 K, there are two different emitting species present, which are not interconverting on the time scale of emission, but whose excited states (HOMO and LUMO) are probably localized on the same parts of the molecule. It seems very likely that the two species are the trans (*E*) and cis (*Z*) isomers, which have significantly different triplet excited-state energies. As noted earlier, the *E*−*Z* photoisomerization process occurs quite rapidly, as monitored by ^{1}H NMR. Thus, in the dilute solutions required for fluorescence spectroscopy, a significant proportion of the *Z* isomer will quickly build up, which probably gives rise to the high-energy set of bands ($E_{00} \approx$ 21100 cm^{-1}), while the *E* isomer emits at longer wavelength ($E_{00} \approx$ 16700 cm^{-1}). In comparison, the triplet state energies of *Z*- and *E*-stilbene itself lie at approximately 19 000 and 17 000 cm^{-1}, respectively, in nonpolar solvents.[20]

Further support for this assignment of the bands comes from the change in the UV−visible absorption spectrum upon irradiation (Figure 10). It can be seen that the spectrum after irradiation displays substantially enhanced absorption in the 360 nm region compared to 400 nm, which must be due to the greater absorbance of the *Z* isomer around 360 nm. This correlates with the strong band observed at this wavelength in the excitation spectrum of the higher-energy emitting species (Figure 9b). We also noted that samples that had been allowed to stand in ambient light for up to 1 h after

(20) *CRC Handbook of Organic Photochemistry*; Scaiano, J. C., Ed.; CRC Press Inc.; Boca Raton, FL, 1989.

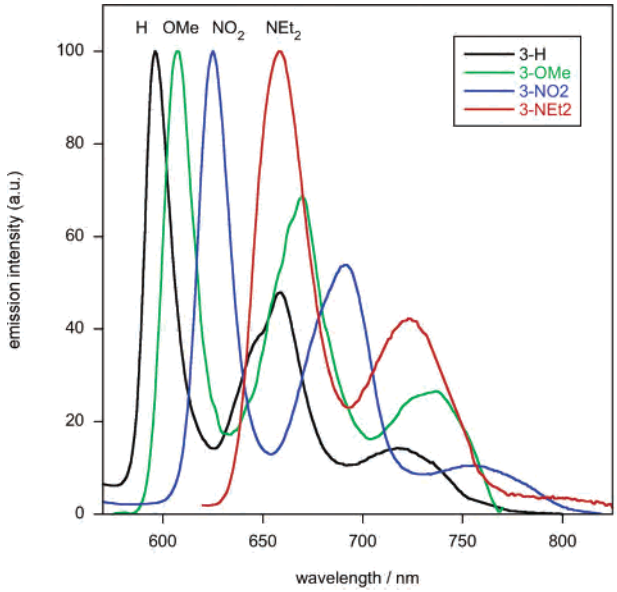

Figure 11. The long wavelength region of the emission spectra of **3-H**, **3-OMe**, **3-NO$_2$**, and **3-NEt$_2$** in an EPA glass at 77 K; λ_{ex} = 400 nm; bandpasses = 2.5 nm. A 450-nm cutoff emission filter was employed to eliminate interference from the second-order scattered light artefact at 800 nm.

preparation, and prior to freezing, displayed a proportionately higher intensity from the short wavelength bands, in line with the build-up of the *Z* isomer. In fact, Thompson et al. have previously observed a second vibrational progression in the case of a related Pt complex containing a methoxy-substituted ppy ligand {[Pt(*C*∧*N*-46dfp-4meopy)(*O*∧*O*-acac)], where 46dfp-4meopyH = 2-(4,6-difluorophenyl)-4-methoxy-pyridine}.[7] This feature was tentatively interpreted in terms of conformational isomerism of the methoxy group with respect to the pyridyl ring. In that case, the two vibrational progressions had similar energy and overlapped. However, the corresponding conformational isomerism of a cis versus trans -CH═CH- double bond represents a much larger difference in molecular structure, and the distinctly different energies of the two sets of bands in the present instance might then be anticipated.

The other three complexes show similar behavior, again with two sets of bands with well-defined vibronic progressions. The positions (wavelengths of band maxima) for the higher-energy bands are similar for all four complexes indicating that, for the *Z* conformation, the styryl substituent R has little influence on the excited-state energy. In contrast, there is a substantial influence of R on the lower-energy set of bands (*E* isomer) (Figure 11). The excited-state energy decreases in the order H > OMe > NO_2 > NEt_2, with E_{00} ranging from ≈ 16 700 cm^{-1} for the unsubstituted styryl complex (**3-H**) to 15 200 cm^{-1} for **3-NEt$_2$**, where the emission extends into the near infrared. This corresponds to a range in λ_{max} from 600 to 658 nm. Thus, the extension of conjugation through introduction of the −CH═CH−Ph double bond leads to a red-shift of 120 nm (λ_{max} = 600 nm for **3-H** compared to 480 nm for [Pt(ppy)(acac)][7]), which can then be further augmented by 58 nm (total of 178 nm) by introducing an amino substituent into the styryl phenyl ring.

The relatively long lifetimes, of the order of 20 μs at 77 K (Table 3), are suggestive of significant intraligand character in the emissive excited state (as predicted by the DFT analysis discussed earlier), as opposed to the shorter lifetimes more typically associated with more purely MLCT states (e.g., values of around 10 μs for the parent complex [Pt(ppy)(acac)] and derivatives[7]). DFT calculations of the lowest energy relaxed triplet state are at least partially consistent with the observed trend in emission energies. Thus, the calculated triplet energies ΔE_{S-T} for Pt(ppy)(acac), follows the order H < OMe < NEt_2 < NO_2.

The somewhat counterintuitive observation that the electron-donating NEt_2 substituent and the electron-withdrawing NO_2 group *both* lead to a lowering of the excited-state energy can be understood in terms of their different effects on HOMO and LUMO, as alluded to earlier. Thus, the NO_2 group has a much greater influence on the LUMO than on the HOMO (see MO diagrams in Figure 7) and stabilizes the former to a larger extent, thus leading to a reduction in the excited-state energy. On the other hand, it is on the HOMO that the NEt_2 group has the greater effect, introducing a substantial contribution from the pendent ring and the more predominant ILCT character discussed above. Thus, it is likely that the HOMO is destabilized more than the LUMO in this case, leading again to a net decrease in the excited-state energy. A similar influence of electron-donating substituents also has been observed in tris chelate iridium complexes Ir(*C*∧*N*-ppy-4-styryl-R)$_3$ (R = OMe, NEt_2), for which the excited-state involves ^{3}IL of the R-styryl ligand.[12]

Conclusion

In summary, a series of luminescent platinum(II) complexes featuring a functionalized ppy ligand were synthesized, and the influence of both the end group and the conjugated bridge on the electronic structure and photophysics was studied.

The X-ray crystal structures of **3-OMe**, **3-NEt$_2$**, **3-NO$_2$**, and **4-OMe** determined and corroborate optimized geometries predicted by DFT. An *E*−*Z* photoizomerization of the styryl group occurs in fluid solution. In all of the complexes, the presence of the styryl -CH═CH- double bond has a direct impact on their emissive properties. In solution at room temperature, the complexes are weakly emissive, due to competitive quenching via the photoizomerization process. We suggest that the observed emissions, which are independent of R, arise from the "Pt(ppy)(acac)" fragment, a fluxional species (C−C half-twisted conformation) being generated in which the styryl pendent group is decoupled from the metal center.

In a frozen glass at 77 K, conformational change can no longer occur, and two emitting species are then present, the starting (*E*) isomer and the accumulated photoproduct (*Z* isomer), which emit over distinctly different wavelength ranges. The emission of all complexes (*E* isomer) are greatly red-shifted {$\Delta\lambda$ = 178 nm compared to [Pt(ppy)(acac)]} and have longer lifetimes compared to those of previously studied (*C*∧*N*)Pt complexes. Such a significant shift is the result of the extension of the π-conjugated system and the electronic

effect of the styryl substituent R. The longer lifetimes observed are indicative of a notable intraligand character. The strong electron-donating amino group and electron-withdrawing nitro group both give rise to red emitters but whose triplet excited states have quite different orbital parentage, according to DFT calculations. The electronic structures of **3-H, 3-OMe**, and **3-NO$_2$** are similar, with a ca. 40% percentage of metal-based HOMO, in agreement with a MLCT/LLCT excited state, whereas for **3-NEt$_2$**, the involvement of a low-lying ^{3}ILCT transition is predominant. A simple modification of the end group allows the introduction of intraligand charge transfer character through the conjugated bridge, accompanied by a further large red-shift in addition to that already induced by the double bond, representing a potentially very powerful strategy for the design of new luminophores.

Experimental Section

General Procedure. All manipulations were performed using Schlenk techniques under an Ar atmosphere. All solvents were dried and purified by standard procedures. NMR spectra were recorded on Bruker DPX-200, AV 300, or AV 500 MHz spectrometers. ^{1}H and ^{13}C chemical shifts are given versus $SiMe_4$ and were determined by reference to residual ^{1}H and ^{13}C solvent signals. Attribution of carbon atoms was based on HMBC, HMQC, and COSY experiments. Cyclic voltammograms were recorded using an EG&G 263 potentiostat in anhydrous DMF containing 0.1 M [^{n}Bu$_4$N][PF$_6$] supporting electrolyte at 20 °C on Pt electrodes with a SCE reference electrode. The ferrocene/ferricinium Cp_2Fe/Cp_2Fe^+ redox couple was used as an internal reference for potential measurements (0.46 V vs SCE). High-resolution mass spectra (HRMS) were performed on a MS/MS ZABSpec TOF at the CRMPO (Centre de Mesures Physiques de l'Ouest) in Rennes. Elemental analyses were performed by Muriel Escadeillas at the CRMPO. UV/vis absorption spectra were recorded using a UVIKON 9413 or Biotek Instruments XS spectrophotometer using quartz cuvettes of 1 cm path length. Steady-state luminescence spectra were measured using a Jobin Yvon FluoroMax-2 or Tau-3 spectrofluorimeter, fitted with a red-sensitive Hamamatsu R928 photomultiplier tube. The spectra shown are corrected for the wavelength dependence of the detector, and the quoted emission maxima refer to the values after correction. The 77 K spectra were acquired uisng an Oxford Instruments Cryostat model DN1704. Luminescence quantum yields were determined using the method of continuous dilution, using [Ru(bpy)$_3$]Cl$_2$ as the standard ($\phi = 0.028$ in air-equilibrated aqueous solution[21]) and correcting for the refractive index. Lifetimes were obtained either by excitation at 355 nm with the third harmonic of a Q-switched Nd:YAG laser and detection of emitted light using an R928 PMT, or by TCSPC following excitation at 405 nm using a laser diode in an Edinburgh Instruments Mini-Tau system.

Density Functional Calculations. The density functional calculations were performed on isolated molecules using the Amsterdam Density Functional (ADF2004.01) program.[22] In this program, scalar relativistic effects are introduced via the zeroth order regular approximation (ZORA) approach to the Dirac equation.[23] A triple-ζ Slater-type (STO) basis set augmented with one set of polarization functions, i.e., the ADF ZORA/TZP basis set was employed for all atoms (H, C, N, O, and Pt). A frozen core approximation was used; the core density is computed relativistically by the Dirac subprogram and is kept frozen during molecular calculations. Core electrons (C.1s), (N.1s), (O.1s) and (Pt.4d) were frozen for carbon, nitrogen, oxygen, and platinum, respectively. Valence electrons spin−orbit effects were not taken into account in our work. The Vosko-Wilk-Nusair functional[24] for the local density approximation (LDA) and the nonlocal corrections respectively for exchange and correlation of Becke and Perdew[25] have been used. The BP86 functional thus used in this work has proven to give good optimized geometries for organometallic species. For the spectroscopic part of this work we used the LB94[26] functional which is better adapted for TDDFT (time-dependent DFT) studies. Molecular orbital plots were generated using the MOLEKEL 4.3 program.[27]

X-ray Crystallography. Single crystals for X-ray diffraction studies were grown by slow diffusion of ethanol in a CH_2Cl_2 solution of complexes **3-OMe**, **4-OMe**, **3-NEt$_2$**, **and 3-NO$_2$** at 20 °C. The samples were studied on an Oxford Diffraction Xcalibur Saphir 3 diffractometer with graphite monochromatized MoKα radiation. The data collection and refinement parameters are presented Table 5. The structures were solved with SIR-97,[28] which reveals the non-hydrogen atoms of the molecules. The whole structures were refined by full-matrix least-squares techniques on F^2, with hydrogens refined using the Riding mode. Structures were solved by Patterson or direct methods. The structures were completed by subsequent difference Fourier techniques and refined by full-matrix least squares on F^2 (SHELXL-97) with initial isotropic parameters.[29] The crystal structures have been deposited at the Cambridge Crystallographic Data Centre and allocated the deposition numbers CCDC-243760 (**3-OMe**), CCDC-256358 (**4-OMe**), CCDC-273291 (**3-NEt$_2$**), and CCDC-297103 (**3-NO$_2$**). These data can be obtained free of charge at www.cccdc.cam.ac.uk/conts/retrieving.html [or from Cambridge Crystallographic Data Centre, 12, Union Road, Cambridge CB2 1EZ; Fax: (internat.) +44−1223/336−033; E-mail: deposit@ccdc.cam.ac.uk].

Syntheses of Chloro-Bridge Dimers [Pt(*C*∧*N*-ppy-4-styryl-R)]$_2$(μ-Cl)$_2$ (2). A Schlenk flask was charged with K_2PtCl_4, the appropriate ligand HC∧N, **1** (3.5 equiv.) and 10 mL of a mixture of 2-ethoxyethanol:water 75:25. The mixture was refluxed for 24h. The precipitate was then washed with water, ethanol, and acetone. The dimers were used without further purification.

(21) Nakamaru, K. *Bull. Chem. Soc. Jpn.* **1982**, *55*, 2697.

(22) (a) Fonseca, C. G.; Snijders, J. G.; Te Velde, G.; Baerends, E. J. *Theor. Chem. Acc.* **1998**, 391. (b) Te Velde, G.; Bickelhaupt,. F. M.; Van Gisbergen, S. A. J.; Fonseca, G. C.; Baerends, E. J.; Snijders, J. G.; Ziegler, T. *J. Comput. Chem.* **2001**, 931. (c) ADF2004.01, Theoretical Chemistry; Scientific Computing and Modelling, Vrije University: Amsterdam, The Netherlands, 2004; http://www.scm.com.

(23) (a) Van Lenthe, E.; Baerends, E. J.; Snijders, J. G. *J. Chem. Phys.* **1993**, *99*, 4597. (b) Van Lenthe, E.; Baerends, E. J.; Snijders, J. G. *J. Chem. Phys.* **1994**, *101*, 9783. (c) E. Van Lenthe, E.; Ehlers, A.; Baerends, E. J. *J. Chem. Phys.* **1999**, *110*, 8943.

(24) Vosko, S. D.; Wilk, L.; Nusair, M. *Can. J. Chem.* **1990**, *58*, 1200.

(25) (a) Becke, A. D. J. *Chem. Phys.* **1986**, *84*, 4524. (b) Becke, A. D. *Phys. Rev. A* **1988**, *38*, 3098. (c) Perdew, J. P. *Phys. Rev. B* **1986**, *33*, 8822. (d) Perdew, J. P. *Phys. Rev. B* **1986**, *34*, 7406. (e) Perdew, J. P.; Wang, Y. *Phys. Rev. B* **1992**, *45*, 3244.

(26) Van Leeuwen, R.; Baerends, E. J. *Phys. Rev A* **1994**, *49*, 2421.

(27) Flükiger, P.; Lüthi, H. P.; Portmann, S.; Weber, J. MOLEKEL4.3; Swiss Center for Scientific Computing: Manno (Switzerland), 2000; http://www.cscs.ch.

(28) Altomare, A.; Burla, M. C.; Camalli, M.; Cascarano, G.; Giacovazzo, C.; Guagliardi, A.; Moliterni, A. G. G.; Polidori, G.; Spagna, R. *Sir97*: A new tool for crystal structure determination and refinement *J. Appl. Crystallogr.* **1998**, *31*, 74.

(29) Sheldrick, G. M. SHELX97-2 Program for Crystal Structure Refinement; University of Göttingen, Germany. 1997. *International Tables for X-ray Crystallography*; Wilson, A. J. C., Ed.; Kluwer Academic Publishers: Dordrecht, 1992; Vol. C. Spek, A.; PLATON. L. *A Multipurpose Crystallographic Tool*, Utrecht University: Utrecht, The Netherlands, 1998.

Table 5. Crystallographic Data for **3-OMe**, **4-OMe**, **3-NEt$_2$**, and **3-NO$_2$**

	3-OMe	4-OMe	3-NEt$_2$	3-NO$_2$
formula	$C_{25}H_{23}NO_3Pt$	$C_{31}H_{35}NO_3Pt$, CH_2Cl_2	$C_{28}H_{30}N_2O_2Pt$	$C_{24}H_{20}N_2O_4Pt$, CH_2Cl_2
FW	580.53	1499.23	1243.26	680.44
cryst syst	monoclinic	monoclinic	monoclinic	monoclinic
space group	*C*2/*c*	*C*2	*P*2$_1$/*c*	*P*2$_1$/*n*
a, Å	18.1706(4)	23.10809)	11.9753(2)	4.8499(2)
b, Å	11.2855(2)	7.0095(2)	30.4584(5)	44.2335(10)
c, Å	21.6821(7)	21.9937(7)	13.2116(2)	11.3166(3)
α, deg	90	90	90	90
β, deg	104.731(5)	117.799	90.2940(10)	106.219(2)
γ, deg	90	90	90	90
V, Å^3	4300.08(18)	3151.30	4818.85(13)	2331.1(1)
Z	8	2	4	4
ρ_{calcd}, g cm^{-1}	1.793	1.58	1.714	1.939
μ (Mo K$_\alpha$), cm^{-1}		0.71073	0.71073	0.71069
temp K	293	293	120(1)	120(1)
F(000)	2256	1488	2448	1320
cryst dimens mm	0.23 × 0.15 × 0.06	0.22 × 0.15 × 0.06	0.15 × 0.12 × 0.02	0.35 × 0.09 × 0.08
θ range, deg	2.62−31.99	2.65−27.51	1.68−27.47	2.97−29.89
index ranges	$-26 \le h \le 19$	$0 \le h \le 29$	$0 \le h \le 15$	$-6 \le h \le 4$
	$-16 \le k \le 16$	$0 \le k \le 9$	$0 \le k \le 39$	$-59 \le k \le 61$
	$-30 \le l \le 32$	$-28 \le l \le 25$	$-17 \le l \le 17$	$-15 \le l \le 15$
no. reflns collcd	33401	3888	11004	19146
no. of indep reflns/*R* int	6479/0.0456	3888/0	11004/0	6228/0.0435
no. of indep reflns with $I > 2\sigma(I)$	3802	2969	9414	5941
GOF (F^2)	0.989	1.011	1.205	0.925
R1 (*F*) ($I > 2\sigma(I)$)	0.0344	0.0425	0.0780	0.0661
R1 (all data)	0.0852	0.0687	0.0935	0.0689
wR2 ($I > 2\sigma(I)$)	0.0699	0.1028	0.1628	0.1394
wR2 (all data)	0.0853	0.1197	0.1700	0.1410
largest diff peak/hole e/Å^3	1.585/−0.786	1.279/−0.999	5.916/−3.543	5.497/−3.141

Synthesis of Pt(*C*∧*N*-ppy-4-styryl-R)(*O*∧*O*)(3−4a,b,c). General Procedure. Dimers **2**, the appropriate diketone (3 equiv) and Na_2CO_3 (10 equiv) were heated in 10 mL of 2-ethoxyethanol at 80 °C overnight. After filtration, the yellow solid was crystallized into a CH_2Cl_2/ethanol mixture.

[Pt(C∧*N*-ppy-4-styryl-H)(*O*∧*O*-acac)] (3-H). (41%). ^{1}H NMR (500 MHz, CD_2Cl_2): 8.91 (d, ^3J = 6 Hz, 1H, Py^6), 7.71 (d, ^4J = 1.5 Hz, 1H, Py^3), 7.65 (d, ^3J = 7.2 Hz, 2H, C_6H_5 *ortho*), 7.59 (d, ^3J = 7.6 Hz, 1H, Ph^6), 7.56 (d, ^3J = 7.6 Hz, 1H, Ph^3), 7.49 (d, ^3J = 17 Hz, 1H, =CH), 7.47 (m, 2H, C_6H_5 *meta*), 7.48−7.41 (m, 1H, C_6H_5 *para*), 7.22 (dd, ^3J = 6.1 Hz, ^4J = 1.8 Hz, 1H, Py^5), 7.22 (td, ^3J = 7.5 Hz, ^3J = 1.3 Hz, 1H, Ph^5), 7.16 (td, ^3J = 7.4 Hz, ^4J = 1.3 Hz, 1H, Ph^4), 7.13 (d, ^3J = 16 Hz, 1H, =CH), 5.54 (s, 1H, CH), 2.05 (s, 3H, Me), 2.03 (s, 3H, Me). ^{13}C [^{1}H] NMR (125 MHz, CD_2Cl_2): 185.9 (C=O), 184.0 (C=O), 167.9 (Py^2), 147.0 (Py^4), 146.8 (Py^6), 144.7 (Ph^2), 139.2 (Ph^1), 135.9 (C_6H_5 ipso), 135.1 (=CH), 130.5 (Ph^6), 129.2 (Ph^5), 128.9 (C_6H_5 *meta* and *para*), 127.3 (C_6H_5 *ortho*), 125.0 (=CH), 123.4 (Ph^4), 122.8 (Ph^3), 118.3 (Py^5), 115.5 (Py^3), 102.3 (CH), 28.0 (CH_3), 26.9 (CH_3). Anal. Calcd for $C_{24}H_{21}NO_2Pt$ C, 52.36; H, 3.85; N, 2.54. Found C, 52.01; H, 3.94; N, 2.67.

[Pt(C∧*N*-ppy-4-styryl-H)(*O*∧*O*-dpm)] (4-H). (yield 32%). ^{1}H NMR (500 MHz, CD_2Cl_2): 8.95 (d, ^3J = 6 Hz, 1H, Py^6), 7.75 (s, 1H, Py^3), 7.66 (m, 3H, Ph and C_6H_5 *ortho*), 7.59 (d, ^3J = 7.6 Hz, 1H, Ph), 7.51 (d, ^3J = 16 Hz, 1H, =CH), 7.45 (m, 4H, C_6H_5 *meta* and *para*), 7.32 (dd, ^3J = 6 Hz, ^4J = 1.7 Hz, 1H, Py^5), 7.24 (td, ^3J = 7.3 Hz, ^3J = 1.2 Hz, 1H, Ph), 7.16 (td, 1H, Ph), 7.16 (d, ^3J = 16 Hz, 1H, =CH), 5.88 (s, 1H, CH), 1.34 (s, 9H, ^{t}Bu), 1.32 (s, 9H, ^{t}Bu). HRMS *m*/*z* 634.2147 [*M*]$^+$ calcd for $C_{30}H_{33}NO_2{}^{195}Pt$ 634.21591. ^{13}C [^{1}H] NMR (125 MHz, CD_2Cl_2): 195.3 (C=O), 193.6 (C=O), 168.1 (Py^2), 146.9 (Py^4), 146.7 (Py^6), 144.2 (Ph^2), 110.2 (Ph^1), 135.9 (C_6H_5 ipso), 134.9 (=CH), 122.8 (Ph^6), 128.9 (C_6H_5 *meta* and *para*), 127.3 (C_6H_5 *ortho*), 125.1 (=CH), 128.9 (Ph$^{4/5}$), 131.0 (Ph^3), 123.3 (Ph$^{5/4}$), 118.4 (Py^5), 115.5 (Py^3), 93.3.3 (CH), 41.5 (^{t}Bu), 40.9 (^{t}Bu), 28.0 (^{t}Bu), 28.4 (^{t}Bu).

[Pt(C∧*N*-ppy-4-styryl-OMe)(*O*∧*O*-acac)] (3-OMe). (yield 40%). ^{1}H NMR (500 MHz, CD_2Cl_2): 8.88 (d, ^3J = 6.2 Hz, 1H, Py^6), 7.69 (d, ^4J = 1.3 Hz, 1H, Py^3), 7.59 (d, ^3J = 8.6 Hz, 2H, C_6H_4), 7.55 (2xd, ^3J = 7 Hz, 2H, Ph^{6}and Ph^3), 7.44 (d, ^3J = 16.2 Hz, 1H, =CH), 7.22 (m, 2H, Py^5 and Ph^5), 7.15 (td, ^3J = 7.5 Hz, 1H, Ph^4), 7.00 (d, ^3J = 16.2 Hz, 1H, =CH), 6.99 (d, ^3J = 8.8 Hz, 2H, C_6H_4), 5.54 (s, 1H, CH), 3.88 (s, 3H, OMe), 2.05 (s, 3H, Me), 2.03 (s, 3H, Me). ^{13}C [^{1}H] NMR (125 MHz, $CDCl_3$): 185.9 (C=O), 184.0 (C=O), 167.7 (Py^2), 160.7 (C_6H_4−C^4), 147.4 (Py^4), 146.7 (Py^6), 144.8 (Ph^2), 139.1 (Ph^1), 134.7 (=CH), 130.5 (Ph^6), 128.8 (C_6H_4−C^2), 128.7 (Ph^5), 128.5 (C_6H_4−C^1) 123.4 (Ph^4), 122.8 (Ph^3), 122.6 (=CH), 118.1 (Py^5), 115.2 (Py^3), 114.3 (C_6H_4−C^3), 102.3 (CH), 55.4 (OMe), 28.0 (CH_3), 26.9 (CH_3). HRMS *m*/*z* 580.1378 [M + H]$^+$ calcd for $C_{25}H_{24}NO_3{}^{195}Pt$ 580.13830.

[Pt(C∧*N*-ppy-4-styryl-OMe)(*O*∧*O*-dpm)] (4-OMe). (yield 35%). ^{1}H NMR (300 MHz, CD_2Cl_2): 8.91 (d, ^3J = 6 Hz, 1H, Py^6), 7.69 (m, 2H, Py^3 and Ph^6), 7.59 (m, 3H, C_6H_4 and Ph^3), 7.43 (d, ^3J = 16 Hz, 1H, =CH), 7.25 (m, 2H, Py^5 and Ph^5), 7.15 (td, ^3J = 7.5 Hz, ^4J = 1 Hz,1H, Ph^4), 6.98 (m, ^3J = 16 Hz, 2H, =CH and C_6H_4), 5.90 (s, 1H, CH), 3.88 (s, 3H, OMe), 1.36 (s, 9H, ^{t}Bu), 1.35 (s, 9H, ^{t}Bu). ^{13}C [^{1}H] NMR (75 MHz, $CDCl_3$): 195.2 (C=O), 193.6 (C=O), 167.9 (Py^2), 160.7 (C_6H_4–C^4), 147.3 (Py^4), 146.6 (Py^6), 144.9 (Ph^2), 140.2 (Ph^1), 134.7 (=CH), 130.9 (Ph^6), 128.9 (Ph^5), 128.8 (C_6H_4−C^2), 128.6 (C_6H_4−C^1), 123.3 (Ph^4), 122.8 (Ph^3), 122.6 (=CH), 118.1 (Py^5), 115.2 (Py^3), 114.3 (C_6H_4−C^3), 93.3 (CH), 55.4 (OMe), 41.5 (^{t}Bu), 41.0 (^{t}Bu), 28.4 (^{t}Bu), 28.1 (^{t}Bu). HRMS: *m*/*z* [M + H]$^+$ 665.2360 calcd for $C_{31}H_{36}NO_3{}^{195}Pt$ 665.2343. Anal. Calcd for $C_{31}H_{35}NO_3Pt$ C, 56.02; H, 5.31; N, 2.11. Found C, 55.79; H, 5.57; N, 1.98.

[Pt(C∧*N*-ppy-4-styryl-NEt$_2$)(*O*∧*O*-acac)] (3-NEt$_2$). (yield 39%). ^{1}H NMR (500 MHz, CD_2Cl_2): 8.82 (d, ^3J = 6.2 Hz, 1H, Py^6), 7.67 (d, ^4J = 1.6 Hz, 1H, Py^3), 7.56 (td, ^3J = 7 Hz, 2H, Ph^{6}and Ph^3), 7.50 (d, ^3J = 8.8 Hz, 2H, C_6H_4), 7.42 (d, ^3J = 16.2 Hz, 1H, =CH), 7.21 (m, 2H, Py^5 and Ph^5), 7.14 (td, ^3J = 7.5 Hz, 1H, Ph^4), 6.88 (d, ^3J = 16.2 Hz, 1H, =CH), 6.73 (d, ^3J = 8.9 Hz, 2H, C_6H_4),

5.54 (s, 1H, CH), 3.45 (q, ^3J = 7 Hz, 4H, Et), 2.04 (s, 3H, Me), 2.02 (s, 3H, Me), 1.23 (t, ^3J = 7 Hz, 3H, Et). ^{13}C [^{1}H] NMR (125 MHz, $CDCl_3$): 185.9 (C═O), 183.9 (C═O), 167.4 (Py^2), 148.8 ($C_6H_4-C^4$), 148.2 (Py^4), 146.4 (Py^6), 145.1 (Ph^2), 138.9 (Ph^1), 135.7 (═CH), 130.4 (Ph^6), 129.0 ($C_6H_4-C^2$), 128.6 (Ph^5), 123.3 (Ph^4), 122.6 ($C_6H_4-C^1$, Ph^3), 118.9 (═CH), 117.6 (Py^5), 114.7 (Py^3), 111.4 ($C_6H_4-C^3$), 102.2 (CH), 44.4 (CH_2), 28.0 (CH_3), 26.9 (CH_3), 12.4 (CH_3). HRMS: *m*/*z* 622.2033 [M + H]$^+$ calcd for $C_{28}H_{31}N_2O_2{}^{195}Pt$ 622.2036. Anal. Calcd for $C_{28}H_{30}N_2O_2Pt$ C, 54.10; H, 4.86; N, 4.51. Found C, 54.23; H, 4.71; N, 4.88.

[Pt(C∧*N*-ppy-4-styryl-NMe$_2$)(*O*∧*O*-dpm)] (4-NMe$_2$). (yield 24%). ^{1}H NMR (300 MHz, CD_2Cl_2): 8.86 (d, ^3J = 6.2 Hz, 1H, Py^6), 7.69 (d, ^4J = 1.6 Hz, 1H, Py^3), 7.64 (d, ^3J = 7.5 Hz, 1H, Ph), 7.57 (d, ^3J = 7.5 Hz, 1H, Ph), 7.53 (d, ^3J = 8.8 Hz, 2H, C_6H_4), 7.44 (d, ^3J = 16 Hz, 1H, ═CH), 7.20 (m, 3H, Py,^{5} $Ph^4$and Ph^5), 6.92 (d, ^3J = 16.2 Hz, 1H, ═CH), 6.77 (d, ^3J = 8.9 Hz, 2H, C_6H_4), 5.87 (s, 1H, CH), 3.06 (s, 6H, NMe_2), 1.33 (s, 9H, ^{t}Bu), 1.32 (s, 9H, ^{t}Bu). Anal. Calcd for $C_{32}H_{38}N_2O_2Pt$ C, 56.71; H, 5.65; N, 4.13. Found C, 56.81; H, 5.50; N, 4.00.

[Pt(C∧*N*-ppy-4-styryl-NO$_2$)(*O*∧*O*-acac)] (3-NO$_2$). (yield 47%). ^{1}H NMR (500 MHz, CD_2Cl_2): 9.01 (d, ^3J = 6.3 Hz, 1H, Py^6), 8.30 (d, ^3J = 8.8 Hz, 2H, C_6H_4), 7.81 (d, ^3J = 8.7 Hz, 2H, C_6H_4), 7.78 (s, 1H, Py^3), 7.59 (2 × d, 2H, Ph^6 and Ph^3), 7.55 (d, ^3J = 16 Hz, 1H, ═CH), 7.31 (m, ^3J = 16 Hz, 2H, ═CH and Py^5), 7.24 (t, ^3J = 7 Hz, 1H, $Ph^{5/4}$), 7.17 (t, ^3J = 7 Hz, 1H, $Ph^{4/5}$), 5.56 (s, 1H, CH), 2.07 (s, 3H, Me), 2.04 (s, 3H, Me). ^{13}C [^{1}H] NMR (125 MHz, DMSO): 186.3 (C═O), 184.0 (C═O), 167.6 (Py^2), 147.6 ($C_6H_4-C^4$), 147.2 (Py^6), 147.0 (Py^4), 144.9 (Ph^2), 143.0 ($C_6H_4-C^1$), 139.3 (Ph^1), 133.7 (═CH), 130.5 (Ph^5), 129.9 (═CH), 129.2 (Ph^4), 128.7 ($C_6H_4-C^2$), 124.7 ($C_6H_4-C^3$), 123.9 (Ph^3 , Ph^6), 120.7 (Py^5), 116.5 (Py^3), 102.9 (CH), 28.5 (CH_3), 27.4 (CH_3). Anal. Calcd for $C_{24}H_{20}N_2O_4Pt\cdot H_2O$ C, 46.98; H, 3.61; N, 4.57. Found C, 46.82; H, 3.48; N, 4.23.

Acknowledgment. This work is supported by COST D035-0010-05. Marc Lepeltier and Mylène Cailleteau are gratefully acknowledged for their experimental assistance. J.A.G.W. thanks the University of Durham, EPSRC, and the Royal Society for equipment grants and Dr. J. Weinstein for assistance with selected 77 K kinetics.

Supporting Information Available: Table of computed dihedral angles of **3-H**, **3-OMe**, **3-NO$_2$**, and **3-NMe$_2$**. This material is available free of charge via the Internet http://pubs.acs.org.

IC0607282